The Astrophysical Journal, 691:738–748, 2009 January 20 doi:10.1088/0004-637X/691/1/738

HIGH-RESOLUTION *K*-BAND SPECTROSCOPY OF MWC 480 AND V1331 Cyg*

Joan R. Najita[1], Greg W. Doppmann[1], John S. Carr[2], James R. Graham[3], and J. A. Eisner[3]
[1] National Optical Astronomy Observatory, 950 N. Cherry Ave., Tucson, AZ 85719, USA
[2] Naval Research Laboratory, Code 7213, Washington, DC 20375, USA
[3] Astronomy Department, UC Berkeley, Berkeley, CA 94720, USA
Received 2008 July 18; accepted 2008 September 15; published 2009 January 19

ABSTRACT

We present high-resolution (R = 25,000–35,000) *K*-band spectroscopy of two young stars, MWC 480 and V1331 Cyg. Earlier spectrally dispersed (R = 230) interferometric observations of MWC 480 indicated the presence of an excess continuum emission interior to the dust sublimation radius, with a spectral shape that was interpreted as evidence for hot water emission from the inner disk of MWC 480. Our spectrum of V1331 Cyg reveals strong emission from CO and hot water vapor, likely arising in a circumstellar disk. In comparison, our spectrum of MWC 480 appears mostly featureless. We discuss possible ways in which strong water emission from MWC 480 might go undetected in our data. If strong water emission is in fact absent from the inner disk, as our data suggest, the continuum excess interior to the dust sublimation radius that is detected in the interferometric data must have another origin. We discuss possible physical origins for the continuum excess.

Key words: circumstellar matter – planetary systems: protoplanetary disks – stars: individual (MWC480, V1331 Cyg) – stars: pre-main sequence

Online-only material: color figures

1. INTRODUCTION

CO overtone emission and hot water emission in the *K*-band are both recognized to probe the hot (> 1500 K) inner gaseous disk surrounding young stars. High spectral resolution studies of CO overtone emission have been used to probe disks surrounding low-mass T Tauri stars, intermediate-mass Herbig Ae stars, and high-mass stars (e.g., Carr et al. 1993; Chandler et al. 1993; Najita et al. 1996; Thi & Bik 2005; Blum et al. 2004; Thi et al. 2005; Berthoud et al. 2007). High-resolution spectroscopy of water emission, both in the *K*-band (Carr et al. 2004; Najita et al. 2000; Thi & Bik 2005) and at longer infrared wavelengths (Salyk et al. 2008; Knez et al. 2007), has also been used to probe the properties of inner gaseous disks.

More recently, it has been argued based on spectrally dispersed interferometric observations that strong water emission is responsible for a significant continuum excess inward of the dust sublimation radius in a disk surrounding a Herbig Ae star (Eisner 2007). Several recent interferometric studies have reported similar evidence for a bright compact source of near-infrared (NIR) emission from Herbig AeBe stars (Eisner et al. 2007; Kraus et al. 2007; Tannirkulam et al. 2008a, 2008b; Isella et al. 2008). The compact continuum emission is attributed by these authors to emission from a gaseous disk interior to the dust sublimation radius. Such a gaseous disk is expected to show significant spectral structure due to emission lines of CO and water and other opacity sources (e.g., Muzerolle et al. 2004; Eisner 2007).

Here we report high-resolution *K*-band spectroscopy of two young stars, MWC 480 and V1331 Cyg. MWC 480 (HD 31648; A3pshe+) is a Herbig Ae star with a stellar mass of 2.3 $M_\odot$ that is surrounded by a rotating disk of gas and dust (Mannings et al. 1997). CO fundamental emission is detected from the source (Blake & Boogert 2004). Spatially resolved millimeter and infrared interferometric studies of the emission from MWC 480 derive an inclination of $i = 26°$–$38°$ for the disk (Simon et al. 2000; Eisner et al. 2004). Spectrally dispersed interferometric observations find evidence for an emission excess located interior to the dust sublimation radius with a spectral shape that suggests emission from hot water vapor (Eisner 2007). Evidence for active accretion in this source includes the presence of associated HH objects and emission lines of Si IV (1394 Å, 1403 Å) that arise from hot accreting gas (Sitko et al. 2008; also Valenti et al. 2000 and Muzerolle et al. 2004).

The other source in our study, V1331 Cyg (LkHa 120), is a pre-main-sequence star in the L988 dark cloud complex. The distance to L988 (see Herbig & Dahm 2006 for a summary) has been estimated as 700–800 pc based on photometry and spectroscopy of nebulous sources in the L988 region (Chavarria 1981; Chavarria & de Lara 1981). Studies of the extinction in the region toward the clouds determine a closer distance for the clouds of 550 pc (Shevchenko et al. 1991) and 500 ± 100 pc (Alves et al. 1998).

Various studies suggest a spectral type for V1331 Cyg (A8-G5) that falls between those of Herbig Ae stars and typical T Tauri stars (Kuhi 1964; Chavarria 1981; Hamann & Persson 1992). V1331 Cyg has an associated molecular outflow (Levreault 1988) and a massive circumstellar disk (0.5 $M_\odot$ assuming 550 pc distance; McMuldroch et al. 1993; see also Weintraub et al. 1991) that is surrounded by a flattened gaseous envelope and a ring of reflection nebulosity viewed at an inclination of $i \sim 30°$. V1331 Cyg is known to show emission in CO overtone bands (Carr 1989). High-resolution *L*-band spectroscopy that shows water and OH emission from V1331 Cyg has also been discussed previously (Najita et al. 2007).

2. OBSERVATIONS

A high-resolution *K*-band spectrum of V1331 Cyg was obtained by one of us (J.R.G.) on 1999 July 3 as part of the

* The data presented herein were obtained at the W. M. Keck Observatory, in part from telescope time allocated to NASA through the agency's scientific partnership with the California Institute of Technology and the University of California. The Observatory was made possible by the generous financial support of the W. M. Keck Foundation.

commissioning of NIRSPEC (McLean et al. 1998), the facility spectrograph on the 10 m Keck 2 telescope. The NIRSPEC echelle and cross-disperser gratings were oriented to image *K*-band orders 33–39 onto the 1024 × 1024 InSb detector array through the N7 blocking filter in four 120 s exposures. Thus, the spectral setup covered 7 spectral regions between 1.93 and 2.31 μm. The spectral regions include the $v = 2$–0 CO overtone lines at the long wavelength end, the Br γ line in the middle of the *K*-band, and numerous lines of water throughout.

Using the 0.″288 (2-pixel) wide slit, $R \simeq 35{,}000$ (8.5 km s^{-1}) spectra were acquired in four beam positions along the 12″ long slit in ∼ 1″ seeing (FWHM *K*-band). During these observations, the internal instrument rotator was on, keeping the slit at a fixed position angle on the sky while the nonequatorially mounted telescope tracked. To remove telluric absorption features, spectra of an early-type star (HR 8146; B2V) were obtained with the same grating setting and at a similar air mass following the V1331 Cyg observations. Spectra of the internal NIRSPEC continuum lamp were taken for flat-fielding, and spectra of internal arc lamps (with emission lines of Argon, Krypton, Xenon, and Neon) were obtained for wavelength calibration.

Similar *K*-band spectra of MWC 480 were obtained on 2007 January 3 with NIRSPEC. The spectral coverage overlapped that of the V1331 Cyg observations by ∼ 75% in orders 33–38. The MWC 480 spectra were acquired through the 0.″432 (3-pixel) wide slit ($R \simeq 24{,}000$; 12.5 km s^{-1} resolution) in *K*-band seeing of 1.″3 (FWHM). Eight exposures of 40 s each were taken in an ABBA nod pattern in which the object was placed at ±6″ from the center of the 24″ long slit. The observations were made in stationary mode. These observations made use of the newer NIRSPEC detector array which has improved performance and fewer bad pixels than the detector used in the 1999 observations. There was some wind shake in the east–west direction (i.e., across the slit) during our observations.

3. DATA REDUCTION

3.1. V1331 Cyg

As a first pass, bad pixels present in the raw object, telluric, and calibration source frames were identified and removed by interpolation using the "fixpix" algorithm within the REDSPEC reduction package (a custom echelle reduction package developed by Kim, Prato, and McLean). Standard IRAF packages (Massey et al. 1992; Massey 1997) were then used to reduce the data. Differencing pairs of exposures taken in different beam positions (e.g., beam A–B and beam C–D) were adequate for sky subtraction. The differenced pairs were then flat-fielded by dividing by the internal continuum lamp frame. Object and telluric calibration spectra in each echelle order were extracted from a spatial profile that was fixed at ±2.5 pixels (±0.″5) about the profile peak. The object and telluric spectra extracted at each nod position were wavelength-calibrated using selected telluric absorption lines (for orders 33, 34, and 35) with wavelengths taken from the HITRAN database (Rothman et al. 1998), and emission lines of Argon, Krypton, Xenon, and Neon from exposures in the internal lamp spectra (for orders 36, 37, and 38).

Telluric features in each of the four nod positions were removed from our object spectra by dividing by the spectrum of the telluric standard star obtained at a similar nod position. Order 35 contained emission from Brγ in our telluric standard. To avoid introducing spurious structure in the object spectra, we divided by the telluric standard to correct for telluric absorption only in regions far from the Brγ line. Residual telluric features are therefore present in the spectral region within ∼ 415 km s^{-1} of the Brγ line center (2.1638–2.1693 μm).

Wavelength-calibrated spectra at different nod positions in each order were summed and then multiplied by a blackbody of 22,000 K to restore the true continuum shape after division by the B2V telluric standard. The flux level in the V1331 spectrum was estimated by the conversion from observed counts in the observations of the standard to its 2MASS *K*-band magnitude ($m_K = 4.48$; 10 Jy), and assuming an equal slit loss between the standard and object observations.

3.2. MWC 480

The MWC480 observations were reduced using a similar procedure. Since these observations made use of the improved NIRSPEC array, there were significantly fewer bad pixels. Thus, bad pixels were individually identified and their values fixed by interpolation using the IRAF task "fixpix." The observations of MWC 480 were taken with a wider slit (3 pixels, 0.″432) and in windy conditions with poor seeing, compared to V1331 Cyg. As a result, the spectral images of MWC 480 and the telluric standard star (HR 1412) that were observed at similar beam positions were summed together without offsets, and their spectra were extracted from a relatively wide (±5 pixels) spectral profile. Good signal-to-noise ratio (S/N) in the exposures of the arc lamps (i.e., Ar, Kr, Xe, and Ne) permitted wavelength calibration of all orders except order 33, where telluric absorption lines were used.

Telluric features in the MWC 480 spectra were removed by dividing by the spectrum of the standard star (HR 1412) obtained at a similar nod position. Several weak stellar absorption lines were present in the standard star spectrum. These were modeled and removed using a stellar synthesis model with $T_{\rm eff} = 7600$ K and $\log g = 3.5$, to match the A7 III spectral type of HR 1412 (Doppmann et al. 2008). Since order 35 contained broad Brγ absorption in our standard, we only divided by the telluric standard to correct for telluric absorption in regions $\gtrsim$ 450 km s^{-1} from the Brγ peak. Thus, telluric features are present in the object spectrum between 2.163 and 2.170 μm.

To restore the true continuum slope in MWC 480, the spectra were multiplied by a 7600 K blackbody after division by the telluric standard. The flux level of MWC 480 was calibrated using the observed counts and 2MASS *K*-band magnitude of HR 1412 ($m_K = 2.880$ or 47 Jy), assuming equal slit losses in the object and telluric observations.

4. RESULTS

Figures 1(a)–1(f) compare the spectra of V1331 Cyg and MWC 480. The spectrum of V1331 Cyg shows significant structure in all orders. In order 33 (Figure 1(a)), strong CO overtone ($v = 2$–0) band head emission is present as are numerous weaker emission lines blueward of the band head. Numerous narrow emission features are present in all other orders, as is strong Brγ emission. The wavelengths of many of the narrow emission features agree with the expected wavelengths of lines identified as water in the infrared sunspot spectrum (Polyansky et al. 1997). In contrast, the MWC 480 spectrum appears mostly featureless in all orders, with the exception of strong Brγ emission in order 35 (Figure 1(c); see also the Appendix).

4.1. Lack of Stellar Photospheric Features from MWC 480

The lack of stellar photospheric features in the MWC 480 spectrum is consistent with the expected strength of such

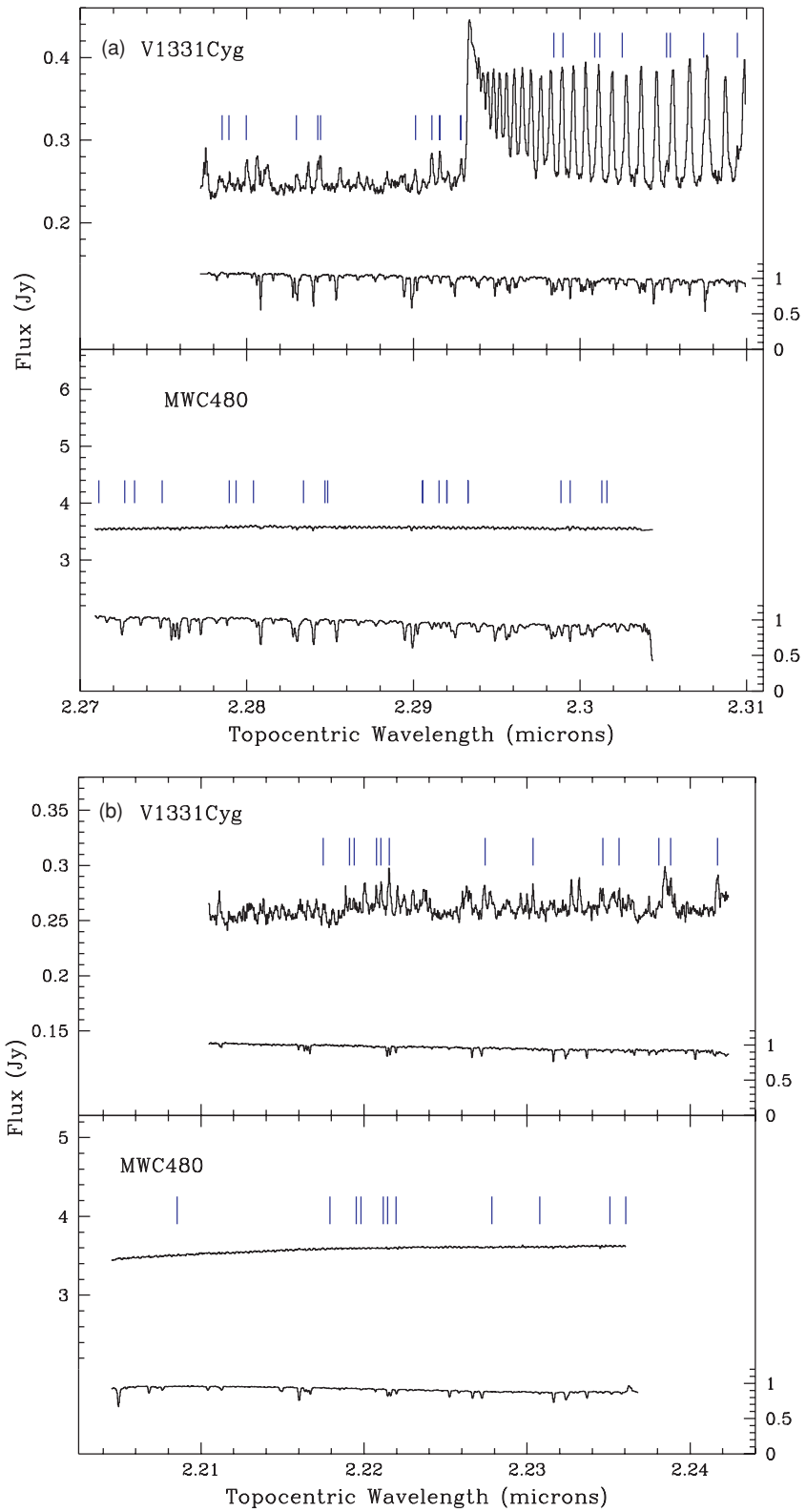

Figure 1. Spectra of V1331 Cyg and MWC 480 in the *K*-band orders 33–38 are shown in Figures 1(a)–1(f), respectively. In each figure, the top panel shows the spectrum of V1331 Cyg (upper histogram) and the corresponding telluric standard spectrum (lower histogram). The telluric spectrum is normalized to unity and plotted against the vertical scale on the right side of the plot. The bottom panel of each figure shows the spectrum of MWC 480 (upper histogram) and its corresponding telluric standard spectrum (lower histogram). In both panels, the positions of known water lines (Polyansky et al. 1997), shifted to the known stellar velocity in the topocentric frame of each object, are also indicated (vertical ticks); this required a velocity shift of -28.7 km s^{-1} and +27.7 km s^{-1} for the lines shown in V1331 Cyg and MWC 480, respectively. In Figure 1(c), the bracketted horizontal lines indicate the regions in which telluric features were not removed; the vertical dashed lines indicate the rest velocity of the Brγ line at the expected stellar radial velocity of the source in the observed frame. False emission features near 1.979 μm and 2.144 μm in the MWC 480 spectrum (indicated by the asterisks) are caused by uncorrected stellar absorption in the A7 telluric standard.

(A color version of this figure is available in the online journal.)

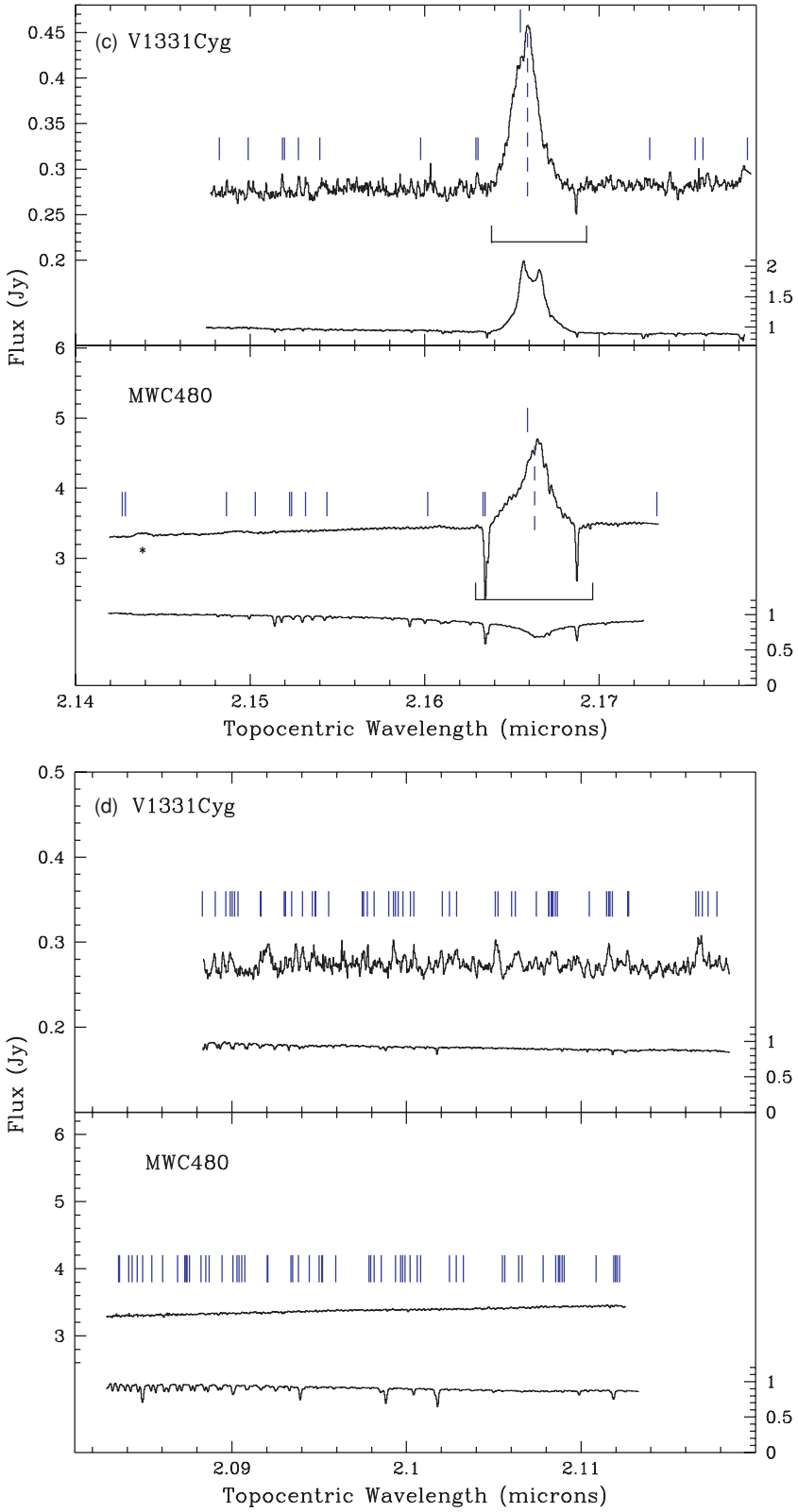

Figure 1. (Continued)

features given the stellar spectral type and photometric veiling estimated for the source. Figure 2 shows the spectral energy distribution (SED) for MWC 480 determined from optical photometry from the Tycho-2 catalog (Høg et al. 2000), the USNO B catalog (Monet et al. 2003), and infrared photometry from 2MASS (Skrutskie et al. 2006) and Morel & Magnenat (1978), dereddened ($A_V = 0.3$, Mannings & Sargent 1997) using an interstellar extinction law with $R_V = 3.1$ (Mathis

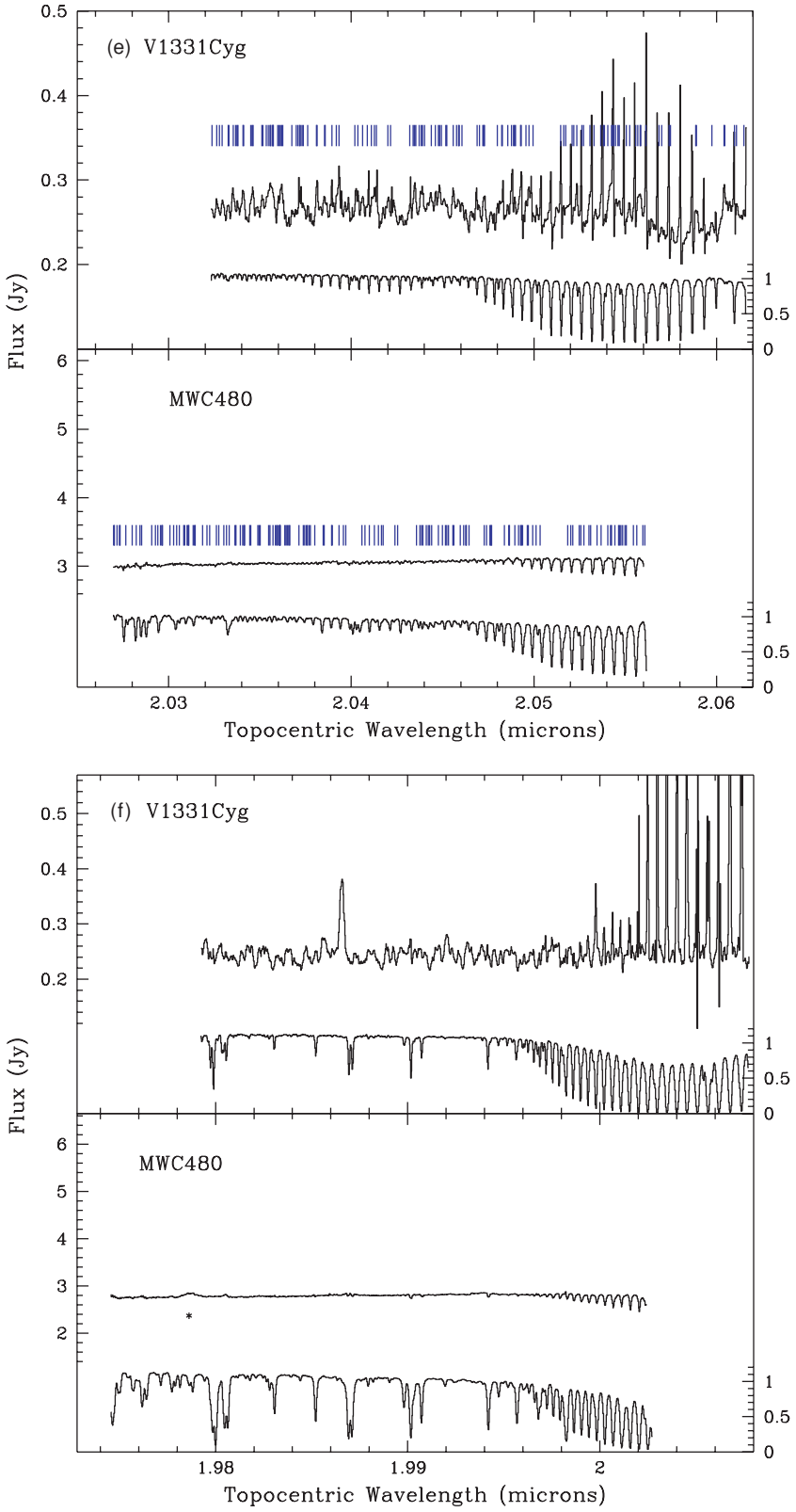

Figure 1. (Continued)

1990). An 8400 K stellar photosphere, consistent with a stellar spectral type of A4 (Simon et al. 2000), provides a good fit to the dereddened optical photometry, assuming a stellar luminosity $L_* = 22\ L_\odot$ and a distance of 170 pc. A distance of 170 pc is within 2σ of the Hipparcos value (van den Ancker et al. 1998). At a distance of 170 pc, dynamical constraints imply a stellar mass of 2 $M_\odot$ for MWC 480 (Simon et al. 2000), consistent with the stellar mass inferred from the pre-main-sequence

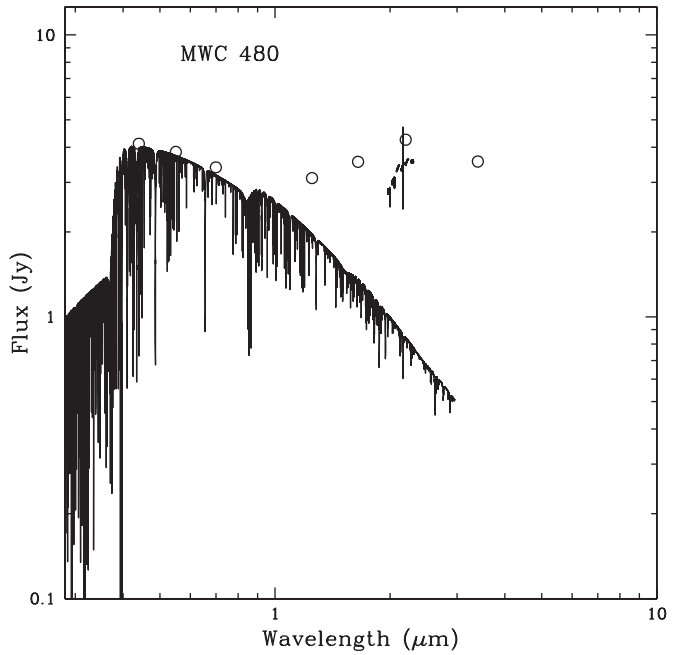

Figure 2. Dereddened SED of MWC 480 (circles) compared with a Kurucz model for $T_{\rm eff} = 8400$ K, $\log g = 4.5$, a stellar luminosity of 22 $L_\odot$, and a distance of 170 pc, assuming an extinction of $A_V = 0.3$. Our flux calibrated NIRSPEC spectrum is also shown. See the text for details.

tracks of Siess et al. (2000) for this luminosity and spectral type.

The 2MASS photometry of MWC 480 shows an infrared SED rising well above the stellar photosphere; the *K*-band excess is $\simeq 4$ times the stellar photospheric continuum. A continuum veiling of this magnitude is consistent with the absence of stellar photospheric features in the NIRSPEC spectra. To estimate the stellar contribution to the spectrum, we generated stellar synthetic spectra using the program MOOG (Sneden 1973) and Hauschildt et al. (1999) model atmospheres. The initial line list was taken from Kurucz (1993), and individual line parameters were adjusted to fit the observed disk-center solar spectrum of Livingston & Wallace (1991).

A synthetic stellar photosphere with $T_{\rm eff} = 8400$ K, $\log g = 4.5$, and $v \sin i = 75$ km s^{-1} predicts weak ($< 2.7\%$ deep) stellar absorption lines in the *K*-band (e.g., Mg I at 2.28143 μm). A stellar rotation velocity of $v \sin i = 75$ km s^{-1} is typical, or even conservative, for a ~ 1 Myr old A-type star, based on rotation statistics found for the Orion OB association (Wolff et al. 2004). With a continuum veiling of $r_K = 4$, the ratio of the continuum excess to the stellar photospheric flux at *K*, these features would be hidden within the noise of our observations (S/N $\sim$ 400), consistent with the absence of absorption features in our spectra of MWC 480.

4.2. CO and Water Emission from V1331 Cyg

In the V1331 Cyg spectrum, the two strongest features blueward of the $v = 2$–0 CO band head have a FWHM of 18–22 km s^{-1}. These lines are blended with weaker water lines, although each feature is dominated by a single strong water line. Isolated CO lines redward of the band head have FWHM $\approx$ 29–35 km s^{-1}. Thus, the water emission lines are narrower than the CO lines, similar to the situation found for other sources such as SVS-13 and DG Tau (Carr et al. 2004; Najita et al. 2000).

CO and water emission from the young star SVS-13 was previously studied by Carr et al. (2004) in the region near the $v = 2$–0 CO band head at 2.3 μm. As discussed in Carr et al. (2004), a major difficulty in modeling NIR water emission is the need for a complete and accurate line list. In their study, Carr et al. (2004) developed a water line list for the 2.3 μm region. They started with the Partridge & Schwenke (1997) theoretical line list and improved the accuracy of both the line positions and strengths. Using the derived line list, they fit the spectrum of SVS-13 with a simple model of a differentially rotating disk.

Here, we adopt the water line list and disk model used by Carr et al. (2004) to model the spectrum of V1331 Cyg. As in Carr et al. (2004), the observed spectrum is modeled under the assumption of Keplerian rotation and thermal level populations (see also Carr et al. 1993; Najita et al. 1996). The disk model parameters include a stellar mass, the projected rotational velocity $v \sin i$ at the inner radius of the emission, the inner and outer radii of the emission, and the temperature and column density distribution for the emitting gas, both parameterized as power laws in radius. The distance and observed velocity shift are additional parameters.

Since the stellar properties of V1331 Cyg (distance, spectral type, extinction) are poorly known, the modeling that we present for the molecular emission from V1331 Cyg is not meant to provide a definitive interpretation of the emission from the source. Instead, the modeling has the limited goal of demonstrating that the observed emission features are consistent with water and CO emission from a differentially rotating disk. A more detailed discussion of the properties of the molecular emission will be presented in a future publication.

In this context, we assume a stellar mass of 1.8 $M_\odot$ which is consistent with estimates for the bolometric luminosity of the source (35–55 $L_\odot$; Hamann & Persson 1992; Shevchenko et al. 1991) and the range of spectral types estimated in the literature (A8–K2; Chavarria 1981; Hamann & Persson 1992). We also assume a distance of 550 pc (Shevchenko et al. 1991; Alves et al. 1998). With the combination of stellar spectral type and extinction preferred by Chavarria (1981; F0 and $A_V = 2.4$) and our assumed stellar luminosity of 12 $L_\odot$, the stellar radius is 2.2 $R_\odot$.

Although the CO and water emission may arise in a vertical temperature inversion region in the disk, for consistency with our limited goal for the modeling in this paper, we ignore the continuum in the modeling. The spectral line emission is therefore assumed to arise in a vertically uniform, continuum-free layer. We also do not include an underlying continuum in fitting the line emission.

The ratios of the water lines blueward of the band head indicates that the water emission is optically thick. Very optically thick emission (a line center optical depth of $\tau \sim 15$ for the water line at 2.2916 μm) is needed to reproduce the strength of the strong water lines (e.g., at 2.2916 μm and 2.2928 μm) relative to the weaker lines (e.g., at 2.2907 μm and 2.2912 μm). Figure 3 shows a fit to the water lines alone using a model of emission from a rotating disk. The model parameters for this fit are a temperature of 1500 K and a line-of-sight column density of 6.8 g cm^{-2}. The assumed parameters correspond to a constant line-of-sight water column density of 1.4×10^{21} cm^{-2} over the emitting region.

The emission lines are narrow, requiring a low projected disk rotational velocity $v \sin i$. Fitting the width of the emission requires a rotational velocity at an inner radius $R_{\rm in}$ of $v \sin i =$

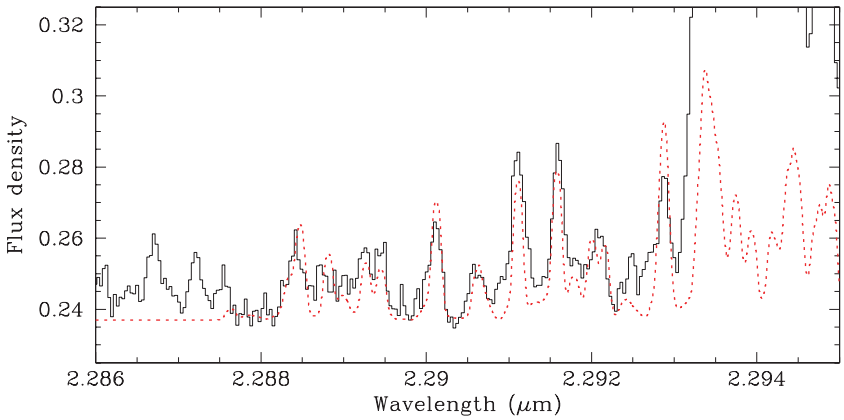

Figure 3. Observed spectrum of V1331 Cyg in the region blueward of the $v = 2$–0 CO band head (black histogram) along with a synthetic disk spectrum that provides a fit to the water emission from this region (dotted line). The water line list covers a limited spectral region, from ~ 2.287 μm to ~ 2.30 μm.

(A color version of this figure is available in the online journal.)

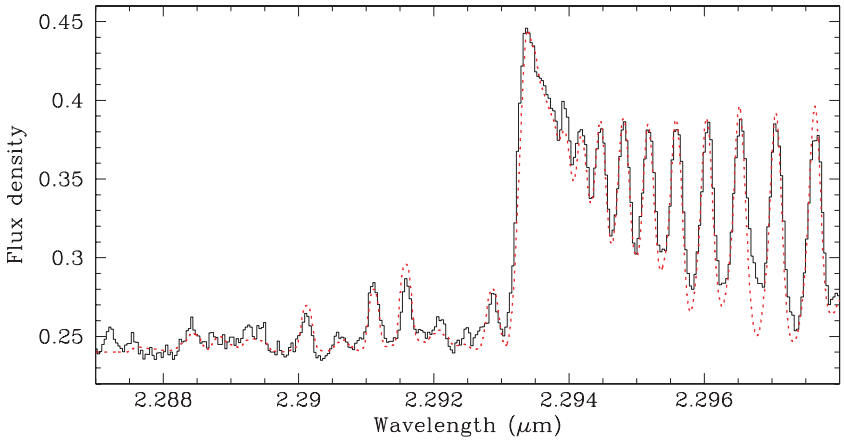

Figure 4. Observed spectrum of V1331 Cyg in the 2.3 μm region (black histogram). A model in which the CO-to-H_2O abundance ratio is much lower than in chemical equilibrium (dotted line) provides a fit to the water and CO emission from this region (see the text for details).

(A color version of this figure is available in the online journal.)

14 km s^{-1} when smoothed to the 8.5 km s^{-1} resolution of the two pixel NIRSPEC slit and assuming no microturbulent broadening. The strength of the emission can be fit assuming an annular emitting region extending from an inner radius of $R_{\rm in} = 5.5\,R_\odot$ to an outer radius of $R_{\rm out} = 5\,R_{\rm in}$. For the assumed stellar mass and the low value of $v \sin i$ required at the inner radius, $R_{\rm in} = 5.5\,R_\odot$ corresponds to a face-on inclination of 3°. The observed emission features are well fit with a topocentric velocity of -29 km s^{-1}, in good agreement with the system radial velocity ($v_{\rm LSR} = -0.7$ km s^{-1}; Levreault 1988; McMuldroch et al. 1993).

We can obtain a reasonable fit to both the CO and water emission using the differentially rotating disk model (Figure 4). The model parameters for this fit are a radial temperature distribution $T = 4100(r/R_{\rm in})^{-0.55}$ and a line-of-sight column density that varies as $\Sigma = 40$ g cm^{-2} $(r/R_{\rm in})^{-0.6}$ between an inner radius of $R_{\rm in} = 2.3\,R_\odot$ and an outer radius of $R_{\rm out} = 15\,R_{\rm in}$. The line-of-sight rotational velocity at $R_{\rm in}$ is $v \sin i = 23$ km s^{-1}, and 4 km s^{-1} of Gaussian microturbulent broadening is assumed throughout. The $v \sin i$ and the microturbulence are jointly constrained by the widths of the isolated water and CO lines, the beating of the CO lines immediately redward of the band head, and the strengths of the CO lines far from the band head compared to the strength of the band head. The 4 km s^{-1} local line broadening used in the fit is in excess of the thermal dispersion of 0.9 km s^{-1} for CO at 2500 K and comparable to the sound speed at that temperature.

Since the relative strength of the CO emission compared to the water emission is much larger than expected for a CO-to-H_2O abundance ratio in chemical equilibrium, the water abundance in the fit is therefore scaled down by a factor of 0.2 relative to its chemical equilibrium value. Because the water emission is less optically thick in this model than in the model shown in Figure 3, the weaker water lines (e.g., at 2.2907 μm and 2.2921 μm) are underfit in the model compared to Figure 3.

In the model, the CO emission forms over radii $\sim$1–7 $R_{\rm in}$, whereas the water emission forms at larger radii $\sim$ 2.2–7.5 $R_{\rm in}$. Since the CO emission extends into smaller disk radii (and higher disk rotational velocities) than the water emission, the water lines are narrower than the CO lines in the synthetic spectrum, in agreement with the observations.

As a caveat, we note that for a source with the properties assumed above, the SED of V1331 Cyg would imply significant veiling, with an optical excess that is 1.7 times the strength of the stellar continuum. Significant veiling at optical wavelengths may help to explain the lack of stellar absorption lines in the optical spectrum of this source (Chavarria 1981). If V1331 Cyg actually experiences little or no optical veiling, the SED would be better fit with a stellar luminosity of 28 $L_\odot$ and a stellar radius of 3.4 $R_\odot$. In such a case $R_{\rm in}$ would have to be larger, and

the other disk model parameters could be modified to produce fits comparable to those shown in Figures 3 and 4. We could fit the water emission alone (the equivalent of Figure 3) by adopting a somewhat smaller disk column density of 4 g cm^{-2} for a larger inner radius of 6.5 $R_\odot$. We could fit both the CO and water emission (the equivalent of Figure 4) by adopting a cooler temperature distribution $T = 3400(r/R_{\rm in})^{-0.55}$ for a larger inner radius of 4 $R_\odot$.

The column density adopted in the modeling is much less than that of either the minimum mass solar nebula or a steady accretion disk that accretes at a rate typical of T Tauri stars. The smaller column density adopted in the modeling may result because the molecular emission arises in a temperature inversion region in the disk atmosphere rather than from the entire vertical column density of an optically thick disk. Alternatively, or in addition, CO and water may not be present throughout (or sufficiently warm enough to emit over) the entire vertical column density of the disk.

The possibility of nonthermal line broadening in the disk atmosphere, as indicated by the shape of the CO overtone emission, is similar to the result obtained by Carr et al. (2004) for the young star SVS-13. In the earlier study, the magnitude of the nonthermal local line broadening was ∼11 km s^{-1} for a Gaussian profile, larger than both the 4 km s^{-1} used here for V1331 Cyg and the line broadening found for the CO band head emission from the Herbig Ae stars WL16 and 1548c27 (Najita et al. 1996). We have previously speculated that nonthermal line broadening is a consequence of turbulence in the disk atmosphere, perhaps produced by the magnetorotational instability.

The large ratio of CO to H_2O emission that we find for V1331 Cyg has also been found for SVS-13 (Carr et al. 2004) and the 6 $M_\odot$ source studied by Thi & Bik (2005). These results have been interpreted as evidence for a reduced H_2O/CO abundance ratio in the disk atmosphere. A reduced H_2O/CO ratio is indeed found for models of strongly irradiated disks surrounding high-mass stars (Thi & Bik 2005). An alternative interpretation might consider the possibility that the water emission is reduced in strength because it arises from a significantly narrower emitting area than we have assumed. This modeling approach has been used in fitting the (spectrally unresolved) rich mid-infrared molecular emission of classical T Tauri stars (Carr & Najita 2008). The near face-on geometry of the V1331 Cyg disk allows for this possibility despite the high velocity resolution of our observations. Detailed theoretical studies of the thermal–chemical properties of disk atmospheres would be needed to determine whether a restricted annular emission region is a reasonable interpretation.

4.3. Lack of Water Emission from MWC 480?

Compared to the rich emission line spectrum of V1331 Cyg, the MWC 480 spectrum appears mostly featureless. The lack of obvious water emission features is perhaps surprising given the results of Eisner (2007). We can use the V1331 Cyg spectrum as a "water emission template" to determine whether velocity broadening by disk rotation or other line-broadening processes can smear out the spectral signature of water in the MWC 480 spectrum.

In Eisner (2007), the observed spectrum and spectrally dispersed visibilities were best fit with a model that included emission from (1) the star, (2) a ring of optically thick dust with a radius 0.28 AU and a temperature of 1200 K, (3) a hot compact component that was modeled as blackbody emission from a ring

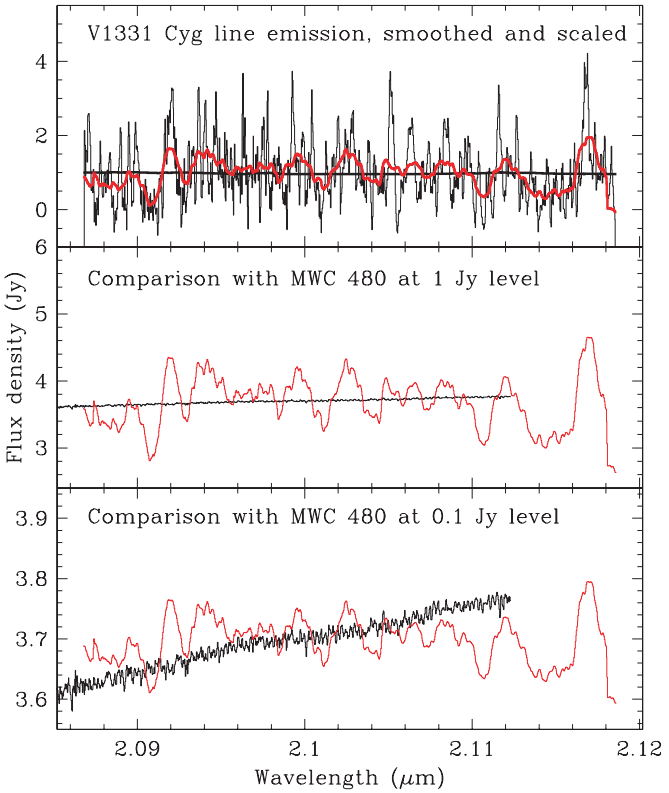

Figure 5. Top: The continuum-subtracted line emission spectrum from V1331 Cyg (black histogram), boxcar smoothed by 36 pixels (or 160 km s^{-1}; red line), twice the width of the CO fundamental emission from MWC 480, and normalized to an average intensity of unity across the order (horizontal line). Middle: The observed spectrum of MWC 480 (black line), compared with the smoothed spectrum of V1331 Cyg from the top panel (red line) which is normalized to the 1 Jy strength of the hot compact continuum in the Eisner (2007) model of MWC 480. Bottom: As in the middle panel, but with the smoothed spectrum of V1331 Cyg (red line) normalized to the 0.1 Jy strength of the water emission in the Eisner (2007) model of MWC 480. Spectral structure similar to that in the smoothed V1331 Cyg spectrum is not present in the MWC 480 spectrum at either the 1 Jy or 0.1 Jy level.

(A color version of this figure is available in the online journal.)

with a radius < 0.1 AU and a temperature of 2410 K, and (4) a ring of gaseous water with a radius of 0.16 AU, a temperature of 2300 K, and a column density of 1.2×10^{19} cm^{-2}. At 2.1 μm, these four components contribute approximately 1 Jy, 1.7 Jy, 1 Jy, and 0.1 Jy, respectively. We can consider two cases: water emission might account for both components (3) and (4) or for component (4) only.

The rotational broadening of the water emission is expected to be 50–70 km s^{-1} based on the stellar mass of MWC 480 (2.3 $M_\odot$), the measured inclination $i = 26°$–$38°$ of the MWC 480 disk (Simon et al. 2000; Eisner et al. 2004), and the disk radius (0.16 AU) of the water emission in the model of Eisner (2007). For the hot compact component, which had a radius $\lesssim$0.1 AU, the expected rotational broadening is somewhat larger, $\gtrsim$60–90 km s^{-1}. Similar velocity widths are found for the CO fundamental emission from MWC 480, which is also believed to originate in the disk. The emission has a FWHM of 62 km s^{-1} for the $J < 9$ lines and ∼ 80 km s^{-1} for the $J > 25$ lines (Blake & Boogert 2004).

To explore the possibility of rotational broadening, we looked at order 36, a spectral order that experiences limited telluric absorption and which is located toward the short wavelength end of the *K*-band where the water emission is expected to become significant. Figure 5 (top panel) shows the (continuum

subtracted) emission line structure in this order of the V1331 Cyg spectrum, scaled in flux so that when it is smoothed to a resolution of $R = 230$ (1300 km s^{-1}; horizontal line) the equivalent pseudo-continuum excess is ~ 1 Jy, the flux of the hot compact component at 2.1 μm. We also show the line emission spectrum (boxcar) smoothed by 36 pixels (or ~ 160 km s^{-1}; red line), larger than the expected rotational broadening for either the water or the hot compact component.

A continuum level of 2.7 Jy is added to the smoothed line emission spectra to bring the total average flux level up to the continuum level of 3.7 Jy found for MWC 480 by Eisner (2007). The middle panel of Figure 5 shows the resulting spectrum (red line) overplotted on the observed MWC480 spectrum in order 36 (black line). Significantly more structure is present than in the MWC 480 spectrum. Thus, rotationally broadened water emission seems unlikely to account for the flux attributed to the hot compact component in the Eisner (2007) model.

The bottom panel of Figure 5 shows an equivalent plot for the case where the pseudo-continuum contributed by the water emission is smaller, 0.1 Jy, the strength of the flux attributed to component (4) in the Eisner (2007) model. In this case as well, the MWC 480 spectrum shows less structure than in the model. Thus, water emission seems unlikely to be present at the level needed to account for the flux attributed to either the hot compact component or the water component of the Eisner (2007) model.

A possible caveat is that the water emission reported by Eisner (2007) may be time variable. The *K*-band flux of MWC 480 is known to vary with time by a modest amount (15%; Sitko et al. 2008; de Winter et al. 2001). However, the strength of the *K*-band continuum in our spectrum is similar to that reported by Eisner (2007), which does not suggest a large spectral variation between the two epochs of observation.

Another possible caveat is that V1331 Cyg is not a good template for the water emission in MWC 480. The water emission in MWC 480 may be much more highly optically thick and line-blanketed, involving much higher water column densities than those considered by Eisner (2007) or than is present in the V1331 Cyg spectrum. The model of water emission used by Eisner (2007) to fit the interferometer observations of MWC 480 is far from being line-blanketed. It is in fact more optically thin than the water emission observed in the V1331 Cyg spectrum. The model parameters used by Eisner (2007), a temperature of 2300 K and a column density of 1.2×10^{19} cm^{-2}, do a reasonable job reproducing the relative fluxes of many of the water lines in the region immediately blueward of the CO overtone band head, with the important exception that the lines at 2.2917 and 2.2928 μm are factors of 2–3 too strong compared to the weaker water lines. This is because the water emission in the Eisner (2007) model is optically thin, whereas the relative fluxes of the water lines in the V1331 Cyg spectrum indicate more optically thick emission.

A more detailed study of possible water emission in MWC 480 would benefit from the development of a reliable water line list for the short wavelength end of the *K* band. This is a subject for future work.

5. DISCUSSION

V1331 Cyg shows a rich spectrum of water emission in the *K* band. In comparison, the *K*-band spectrum of MWC 480 shows little emission from water or any other spectral lines. The nondetection of water emission is consistent with the absence of CO overtone emission from MWC 480: all sources of *K*-band water emission reported in the literature also show CO overtone emission (Carr et al. 2004; Thi & Bik 2005; Najita et al. 2000; this paper; see also van Boekel 2007).

The spectral shape of the low-resolution Keck interferometric spectrum of MWC 480 (Eisner 2007) is consistent with the lack of water emission features in the high-resolution spectrum of MWC 480. One difference between the low-resolution spectrum of MWC 480 and the spectrum of a source like SVS-13, which is known to show strong water emission, is that at low spectral resolution SVS-13 shows an upturn in the continuum at both the long- and short-wavelength ends of the *K* band. The spectral shape is interpreted as a signature of water emission from the 1.9 μm and 2.7 μm water bands (Carr et al. 2004). In contrast, the spectrum of MWC 480 shows a significant excess over the continuum at the short wavelength end, while the long-wavelength spectrum is consistent with continuum emission only. To fit the data, Eisner (2007) used hot (2300 K) water emission, which produces relatively more flux at the short-wavelength end of the *K* band than would cooler material.

Although MWC 480 shows neither CO overtone nor water emission, there is evidence for disk gas inward of the dust sublimation radius, as would be expected for a source with a significant outer disk (0.02–0.2 $M_\odot$; Mannings & Sargent 1997; Hamidouche et al. 2006) that is believed to be accreting (Sitko et al. 2008). The high-*J* CO fundamental emission from MWC 480 has line wings extending to ~ 80 km s^{-1} (Blake & Boogert 2004). At an inclination of $i = 26°$–$38°$ and a stellar mass of 2.3 $M_\odot$, this implies that the CO fundamental emission extends to within 0.06–0.12 AU for Keplerian rotation, well within the dust sublimation radius of ~ 0.28 AU (Eisner 2007). While there is clearly gas within the dust sublimation radius of MWC 480, the CO and water column densities and/or the temperature there are perhaps too low to produce CO overtone or water emission.

The presence of CO fundamental emission, accompanied by the absence of CO overtone and *K*-band water emission, is the situation commonly found for classical T Tauri stars. CO fundamental emission is detected from nearly all accreting T Tauri stars studied (Najita et al. 2003), whereas CO overtone and *K*-band water emission are restricted to the high accretion rate systems (Najita et al. 2000, 2007). CO overtone emission is also rare among high-mass stars (Hanson et al. 1997).

In contrast, models of gaseous inner disks that assume LTE molecular abundances and include NIR opacity sources such as water, CO, and H^- predict prominent NIR spectral structure from Herbig Ae disks. In Muzerolle et al. (2004), a dust-free gaseous inner disk is found to be capable of producing a significant *K*-band flux. At a nominal Taurus distance of 140 pc, an excess of ~ 1 Jy in the *K* band (the flux of the hot compact continuum in MWC 480) can be produced in disks with accretion rates of $\sim 10^{-8}$ $M_\odot$ yr^{-1}. Although such a model can plausibly account for the magnitude of the compact excess that is observed in MWC 480, the excess is also predicted to show strong *K*-band emission features of CO and water, which are not observed.

The models further predict prominent CO and water features over a wide range in accretion rate (10^{-8} to 10^{-5} $M_\odot$ yr^{-1}; Muzerolle et al. 2004; Calvet et al. 1991). Emission is predicted at lower accretion rates and absorption at higher accretion rates. The relative rarity of CO overtone and water features (in emission or absorption) from Herbig Ae stars suggests that something is missing from the assumed physical–thermal–chemical structure of the disk in these models. Possibilities

include non-LTE abundances, photodissociation, and missing sources of continuum opacity and ionization.

If water emission does not appear to be responsible for the excess detected inward of the dust sublimation radius in MWC 480, what is the origin of the excess? The lack of molecular emission might be explained by the presence of a competing source of continuum opacity that produces the hot compact excess. Possible additional opacity sources are high temperature condensates, H^-, and free–free emission. Materials such as corundum (Al_2O_3), hibonite ($CaAl_{12}O_{19}$), perovskite ($CaTiO_3$), and gehlenite ($Ca_2Al_2SiO_7$) are found in CI chondrites and have high sublimation temperatures of 1640–1800 K (Posch et al. 2007). However, they have poor *K*-band emission efficiencies $Q_{\rm abs} \lesssim 10^{-3}$ (Henning et al. 1999[4]; also B. Sargent 2008, private communication), which makes it less likely that they will contribute significantly to the *K*-band opacity.

Graphite grains, often invoked to explain the 2175 Å bump in the interstellar extinction curve, also have a high sublimation temperature (> 2000 K) at interstellar pressures (Krügel 2003; Salpeter 1977). However, graphite may be destroyed by processes such as chemisputtering at much lower temperatures ~1200 K (Lenzuni et al. 1995; Duschl et al. 1996). So it is unclear whether it can explain the observed hot, compact excess in MWC 480. Another possibility is that solids disappear through sublimation over a finite range in temperature (and disk radius). For example, in considering the balance between the solid and gas phases for magnesium–iron silicates, Duschl et al. (1996) found that the gas and dust phases coexist over a range in temperature, with a fraction of silicates surviving to temperatures ~2100 K at the densities of the inner disk region (~ 0.1 AU). Aluminum–calcium-silicates may be sustained to somewhat higher temperatures. Detailed modeling of this kind may be needed to understand the conditions under which dust grains may contribute a modest residual continuum opacity in the high temperature inner regions of disks.

A significant free–free continuum flux requires a significant electron abundance in the inner disk. For optically thin free–free emission from a 10^4 K gas in a cylindrical volume that is $r = 0.1$ AU in radius and $h = 0.1r$ in height, an electron density of $n_e \sim 3 \times 10^{11}$ cm^{-3} is needed to produce a continuum flux of ~1 Jy at a distance of 140 pc. In comparison, for a steady accretion disk accreting at the rate $\dot{M}$, the disk column density is $\Sigma = \dot{M}/3\pi\alpha c_s H$ where α is the viscosity parameter, and c_s is the sound speed. The quantity $H = c_s/\Omega$ is the disk scale height, where Ω is the Keplerian angular velocity. The average disk density can be estimated as $\bar{n}_{\rm H} = \Sigma/\mu m_H H \simeq 5 \times 10^{15}$ cm^{-3} for an accretion rate of 10^{-7} $M_\odot$ yr^{-1}, a stellar mass $M_* = 2.3$ $M_\odot$, and a viscosity parameter $\alpha = 0.01$. Comparing these densities, we require a high average electron fraction in the disk $\bar{x}_e = n_e/\bar{n}_{\rm H} \sim 10^{-4}$ in order to produce a ~ 1 Jy free–free continuum flux from a disk accreting at 10^{-7} $M_\odot$ yr^{-1}.

Continuum opacity from H^- is another possibility. At a column density $N_{\rm H} > 10^{26}$ cm^{-2} and temperature $T > 4000$ K, the H^- continuum optical depth $\tau > 1$ in chemical equilibrium (e.g., Najita et al. 1996). Such warm temperatures are expected for inner disks with accretion rates $> 10^{-7} M_\odot$ yr^{-1}; the midplane H^- opacity is expected to become significant under these conditions (Muzerolle et al. 2004). The possibility of a high H^- opacity at a column density $N_{\rm H} > 10^{26}$ cm^{-2} is also noted by Thi & Bik (2005). Further studies of the gas temperature, electron fraction, and H^- abundance expected for the specific conditions in the inner region of the MWC 480 disk would be useful to sort out these possibilities.

[4] http://www.astro.uni-jena.de/Laboratory/OCDB/oxsul.html

6. SUMMARY AND FUTURE DIRECTIONS

Several recent interferometric studies have reported evidence for a bright compact source of NIR emission interior to the dust sublimation radius in Herbig AeBe stars (Eisner 2007; Eisner et al. 2007; Kraus et al. 2007; Tannirkulam et al. 2008a, 2008b; Isella et al. 2008; Akeson et al. 2005). The compact continuum emission has been attributed to emission from a gaseous disk and variously modeled as hot water emission (Eisner 2007), a uniform disk of a given flux (Tannirkulam et al. 2008a), a 2500 K blackbody (Isella et al. 2008), or an optically thick disk that reradiates away the accretion energy (Kraus et al. 2007). Such a gaseous disk is expected to show significant spectral structure (e.g., Muzerolle et al. 2004; Eisner 2007).

Our study of MWC 480 does not reveal any significant spectral structure in the *K*-band spectrum of the source, suggesting that the compact excess is produced by a continuum process (e.g., high temperature condensates, H^-, or free–free emission) rather than by line emission. It would be interesting to carry out similar studies for other sources with compact continuum excesses in order to determine if the results obtained here for MWC 480 apply more broadly to other sources with compact continuum excesses.

Given its narrow emission lines, V1331 Cyg is a good template for warm water emission from a circumstellar disk. The emission spectrum may also be useful in constructing a reliable water line list for the *K* band.

We thank Ben Sargent and Michael Meyer for helpful insights on high temperature condensates. Financial support for this work was provided by the NASA Origins of Solar Systems program (NNH07AG51I) and the NASA Astrobiology Institute under Cooperative Agreement No. CAN-02-OSS-02 issued through the Office of Space Science. This work was also supported by the Life and Planets Astrobiology Center (LAPLACE). Basic research in infrared astronomy at the Naval Research Laboratory is supported by 6.1 base funding. This publication makes use of data products from the Two Micron All Sky Survey, which is a joint project of the University of Massachusetts and the Infrared Processing and Analysis Center/California Institute of Technology, funded by the National Aeronautics and Space Administration and the National Science Foundation. The authors wish to recognize and acknowledge the very significant cultural role and reverence that the summit of Mauna Kea has always had within the indigenous Hawaiian community. We are most fortunate to have the opportunity to conduct observations from this mountain.

APPENDIX

Brγ EMISSION

As noted in Section 3, the spectra of V1331 Cyg and MWC 480 were not corrected for telluric absorption in the region immediately surrounding the Brγ line because of the presence of Brγ absorption in the telluric standard. Nevertheless we can deduce a few basic features of the Brγ emission present in both spectra. The emission is broad in both V1331 Cyg and MWC 480, with FWZI widths of 550 km s^{-1} and 640 km s^{-1}, respectively. The emission equivalent width and integrated line flux are approximately −9.8 Å and 1.8×10^{-16} W m^{-2},

respectively, for V1331 Cyg and approximately −6.9 Å and 1.5×10^{-15} W m^{-2}, respectively, for MWC 480.

The emission centroids are blueshifted from their systemic velocities by −12.7 km s^{-1} for V1331 Cyg and −6.8 km s^{-1} for MWC 480. Similarly, blueshifted Brγ centroids are found for lower mass T Tauri stars (e.g., Najita et al. 1996; Folha & Emerson 2001). In the context of T Tauri stars, blueshifted Brγ centroids are taken to indicate that the Brγ emission arises in gas infalling in a stellar magnetosphere (e.g., Muzerolle et al. 1998). The line flux and emission centroid measured for V1331 Cyg are similar to the values reported earlier for the same object. We earlier found a line flux of 2.3×10^{-16} W m^{-2} and an emission centroid blueshifted by −12 km s^{-1} (Najita et al. 1996).

REFERENCES

Akeson, R. L., et al. 2005, ApJ, 622, 440
Alves, J., Lada, C. J., Lada, E. A., Kenyon, S. J., & Phelps, R. 1998, ApJ, 506, 292
Berthoud, M. G., Keller, L. D., Herter, T. L., Richter, M. J., & Whelan, D. G. 2007, ApJ, 660, 461
Blake, G. A., & Boogert, A. C. A. 2004, ApJ, 606, L73
Blum, R. D., Barbosa, C. L., Damineli, A., Conti, P. S., & Ridgway, S. 2004, ApJ, 617, 1167
Calvet, N., Patiño, A., Magris, G., & D'Alessio, P. 1991, ApJ, 380, 617
Carr, J. S. 1989, ApJ, 345, 522
Carr, J. S., & Najita, J. R. 2008, Science, 319, 1504
Carr, J. S., Tokunaga, A. T., & Najita, J. 2004, ApJ, 603, 213
Carr, J. S., Tokunaga, A. T., Najita, J., Shu, F. H., & Glassgold, A. E. 1993, ApJ, 411, L37
Chandler, C. J., Carlstrom, J. E., Scoville, N. Z., Dent, W. R. F., & Geballe, T. R. 1993, ApJ, 412, L71
Chavarria, K. C. 1981, A&A, 101, 105
Chavarria, K. C., & de Lara, E. 1981, Rev. Mex. Astron. Astrofis., 6, 159
de Winter, D., van den Ancker, M. E., Maira, A., Thé, P. S., Djie, H. R. E. T. A., Redondo, I., Eiroa, C., & Molster, F. J. 2001, A&A, 380, 609
Doppmann, G. W., Najita, J. R., & Carr, J. S. 2008, ApJ, 685, 298
Duschl, W. J., Gail, H.-P., & Tscharnuter, W. M. 1996, A&A, 312, 624
Eisner, J. A. 2007, Nature, 447, 562
Eisner, J. A., Chiang, E. I., Lane, B. F., & Akeson, R. L. 2007, ApJ, 657, 347
Eisner, J. A., Lane, B. F., Hillenbrand, L. A., Akeson, R. L., & Sargent, A. I. 2004, ApJ, 613, 1049
Folha, D. F. M., & Emerson, J. P. 2001, A&A, 365, 90
Hamann, F., & Persson, S. E. 1992, ApJ, 394, 628
Hamidouche, M., Looney, L. W., & Mundy, L. G. 2006, ApJ, 651, 321
Hanson, M. M., Howarth, I. D., & Conti, P. S. 1997, ApJ, 489, 698
Hauschildt, P. H., Allard, F., & Baron, E. 1999, ApJ, 512, 377
Henning, Th., Il'in, V. B., Krivova, N. A., Michel, B., & Voshchinnikov, N. V. 1999, A&A Suppl., 136, 405
Herbig, G. H., & Dahm, S. E. 2006, AJ, 131, 1530
Høg, E., et al. 2000, A&A, 355, L27
Isella, A., Tatulli, E., Natta, A., & Testi, L. 2008, A&A, 483, L13
Knez, C., et al. 2007, American Astronomical Society Meeting Abstracts 211, No. 50.05
Kraus, S., Preibisch, T., & Ohnaka, K. 2007, A&A, 466, 649
Krügel, E. 2003, The Physics of Interstellar Dust (Bristol: Institute of Physics)
Kuhi, L. V. 1964, ApJ, 140, 1409
Kurucz, R. 1993, in ATLAS9 Stellar Atmosphere Programs and 2 km/s grid, Kurucz CD-ROM No. 13, (Cambridge, MA: Smithsonian Astrophysical Observatory), 13
Lenzuni, P., Gail, H.-P., & Henning, Th. 1995, ApJ, 447, 848
Levreault, R. M. 1988, ApJ, 330, 897
Livingston, W., & Wallace, L. 1991, NSO Technical Report, (Tucson: National Solar Observatory, National Optical Astronomy Observatory)
Mannings, V., Koerner, D. W., & Sargent, A. I. 1997, Nature, 388, 555
Mannings, V., & Sargent, A. I. 1997, ApJ, 490, 792
Massey, P. 1997, A User's Guide to CCD reductions with *IRAF* (Tucson, AZ: National Optical Astronomy Observatory), http://iraf.noao.edu/iraf/ftp/iraf/docs/ccduser2.ps.Z
Massey, P., Valdes, F., & Barnes, J. 1992, A Users's Guide to Reducing Slit Spectra with *IRAF* (Tucson, AZ: National Optical Astronomy Observatory), http://iraf.noao.edu/iraf/ftp/iraf/docs/spect.ps.Z
Mathis, J. S. 1990, ARA&A, 28, 37
McLean, I. S., et al. 1998, Proc. SPIE, 3354, 566
McMuldroch, S., Sargent, A. I., & Blake, G. A. 1993, AJ, 106, 2477
Monet, D. G., et al. 2003, AJ, 125, 984
Morel, M., & Magnenat, P. 1978, A&AS, 34, 477
Muzerolle, J., D'Alessio, P., Calvet, N., & Hartmann, L. 2004, ApJ, 617, 406
Muzerolle, J., Hartmann, L., & Calvet, N. 1998, AJ, 116, 2965
Najita, J. R., Carr, J. S., Glassgold, A. E., Shu, F. H., & Tokunaga, A. T. 1996, ApJ, 462, 919
Najita, J. R., Carr, J. S., Glassgold, A. E., & Valenti, J. A. 2007, in Protostars and Planets V, ed. B. Reipurth, D. Jewitt, & K. Keil (Tucson: Univ. of Arizona), 507
Najita, J., Carr, J. S., & Mathieu, R. D. 2003, ApJ, 589, 931
Najita, J. R., Edwards, S., Basri, G., & Carr, J. 2000, in Protostars and Planets IV, ed. V. Mannings, A. P. Boss, & S. S. Russell (Tucson: Univ. of Arizona), 457
Partridge, H., & Schwenke, D. W. 1997, J. Chem. Phys., 106, 4618
Polyansky, O. L., Zobov, N. F., Viti, S., Tennyson, J., Bernath, P. F., & Wallace, L. 1997, ApJ, 489, L205
Posch, Th., Mutschke, H., Trieloff, M., & Henning, Th. 2007, ApJ, 656, 615
Rothman, L. S., et al. 1998, J. Quant. Spectrosc. Radiat. Transfer, 60, 665
Salpeter, E. E. 1977, ARA&A, 15, 267
Salyk, C., Pontoppidan, K. M., Blake, G. A., Lahuis, F., van Dishoeck, E. F., & Evans, N. J., II. 2008, ApJ, 676, L49
Shevchenko, V. S., Yakulov, S. D., Hambarian, V. V., & Garibjanian, A. T. 1991, AZh, 68, 275
Siess, L., Dufour, E., & Forestini, M. 2000, A&A, 358, 593
Simon, M., Dutrey, A., & Guilloteau, S. 2000, ApJ, 545, 1034
Sitko, M. L., et al. 2008, ApJ, 678, 1070
Skrutskie, M. F., et al. 2006, AJ, 131, 1163
Sneden, C. 1973, PhD thesis, University of Texas at Austin
Tannirkulam, A., et al. 2008a, ApJ, 677, L51
Tannirkulam, A., et al. 2008b, ApJ, 689, 513
Thi, W.-F., & Bik, A. 2005, A&A, 438, 557
Thi, W.-F., van Dalen, B., Bik, A., & Waters, L. B. F. M. 2005, A&A, 430, L61
Valenti, J. A., Johns-Krull, C. M., & Linsky, J. L. 2000, ApJS, 129, 399
van Boekel, R. 2007, Nature, 447, 535
van den Ancker, M. E., de Winter, D., & Tjin A Djie, H. R. E. 1998, A&A, 330, 145
Weintraub, D. A., Sandell, G., & Duncan, W. D. 1991, ApJ, 382, 270
Wolff, S. C., Strom, S. E., & Hillenbrand, L. A. 2004, ApJ, 601, 979